doi:10.1016/j.jmb.2009.10.072 J. Mol. Biol. (2010) 395, 430–443

JMB

Available online at www.sciencedirect.com

ScienceDirect

ELSEVIER

Molecular Basis for the Recognition and Cleavages of IGF-II, TGF-α, and Amylin by Human Insulin-Degrading Enzyme

Qing Guo[1], Marika Manolopoulou[1], Yao Bian[1], Alexander B. Schilling[2] and Wei-Jen Tang[1]*

[1]*Ben-May Department for Cancer Research, The University of Chicago, 929 East 57th Street, Chicago, IL 60637, USA*

[2]*Proteomics and Informatics Services Facility, University of Illinois at Chicago, 835 South Wolcott Avenue, Chicago, IL 60612, USA*

Received 8 June 2009; received in revised form 26 October 2009; accepted 27 October 2009
Available online 5 November 2009

Insulin-degrading enzyme (IDE) is involved in the clearance of many bioactive peptide substrates, including insulin and amyloid-β, peptides vital to the development of diabetes and Alzheimer's disease, respectively. IDE can also rapidly degrade hormones that are held together by intramolecular disulfide bond(s) without their reduction. Furthermore, IDE exhibits a remarkable ability to preferentially degrade structurally similar peptides such as the selective degradation of insulin-like growth factor (IGF)-II and transforming growth factor-α (TGF-α) over IGF-I and epidermal growth factor, respectively. Here, we used high-accuracy mass spectrometry to identify the cleavage sites of human IGF-II, TGF-α, amylin, reduced amylin, and amyloid-β by human IDE. We also determined the structures of human IDE–IGF-II and IDE–TGF-α at 2.3 Å and IDE–amylin at 2.9 Å. We found that IDE cleaves its substrates at multiple sites in a biased stochastic manner. Furthermore, the presence of a disulfide bond in amylin allows IDE to cut at an additional site in the middle of the peptide (amino acids 18–19). Our amylin-bound IDE structure offers insight into how the structural constraint from a disulfide bond in amylin can alter IDE cleavage sites. Together with NMR structures of amylin and the IGF and epidermal growth factor families, our work also reveals the structural basis of how the high dipole moment of substrates complements the charge distribution of the IDE catalytic chamber for the substrate selectivity. In addition, we show how the ability of substrates to properly anchor their N-terminus to the exosite of IDE and undergo a conformational switch upon binding to the catalytic chamber of IDE can also contribute to the selective degradation of structurally related growth factors.

Keywords: metalloprotease; X-ray crystallography; substrate specificity; insulin-degrading enzyme; mass spectrometry

Edited by I. Wilson

Introduction

Insulin-degrading enzyme (IDE) is a 110-kDa zinc metalloprotease that belongs to the M16A family (EC 3.4.24.56, insulysin, or insulinase).[1,2] Similar to other M16 family proteases, IDE has a conserved inverted zinc-binding sequence HEXXH in which the two histidines are involved in zinc ion coordination and one glutamate residue is involved in catalytic water activation.[1–4] Recent structural analysis revealed that human IDE consists of two roughly equally sized N- and C-terminal domains (IDE-N and IDE-C).[3] IDE-N and IDE-C are homologous to each other and have an αβαβα-roll

*Corresponding author. E-mail address: wtang@uchicago.edu.

Abbreviations used: IDE, insulin-degrading enzyme; IGF, insulin-like growth factor; IGF-II, insulin-like growth factor-II; TGF-α, tumor growth factor-α; EGF, epidermal growth factor; Aβ, amyloid-β; MS, mass spectrometry; LC, liquid chromatography; TOF, time of flight; Q-TOF, quadruple time of flight; MALDI, matrix-assisted laser desorption/ionization; FT-ICR, Fourier transform ion cyclotron resonance; TCEP, tris(2-carboxyethyl) phosphine; PDB, Protein Data Bank.

structure, shared among proteases within the M16 family, which include mitochondrial processing peptidase, pitrilysin, and mitochondrial presequence peptidase.[5–7] IDE-N and IDE-C are joined by an extended 28-aa loop, and together, they form an enclosed chamber to selectively enclose and cleave certain peptides. IDE was recently described as a prototypical cryptidase because of its ability to use a sizable catalytic chamber (crypt) to selectively recognize peptides targeted for proteolysis.[1]

Since the discovery of IDE based on its ability to rapidly degrade insulin, IDE was shown to play a major role in the degradation and clearance of insulin *in vivo*.[1,2,8,9] This is consistent with the observation that IDE gene knockout mice have an elevated level of insulin and develop symptoms of diabetes, while single nucleotide polymorphisms of the IDE gene are associated with type 2 diabetes in humans.[10,11] IDE also plays a role in preventing formation of amyloid deposits by degrading amyloid-β (Aβ), a key peptide for the development of Alzheimer's disease.[1,10,12–14] Outside of insulin and Aβ, several short peptides with molecular masses of 3–10 kDa have been shown to serve as substrates of IDE, such as insulin-like growth factor (IGF)-II,[15,16] amylin,[3] glucagon, transforming growth factor-α (TGF-α),[17] and atrial natriuretic peptide.[18]

The structural analysis of substrate-bound IDE has revealed several unique features of how IDE selectively degrades certain bioactive peptides.[1–3,19–21] IDE has a catalytic chamber with a total volume of approximately 16,000 Å^3. The unique size of this chamber allows the enzyme to preferentially cleave peptides smaller than 80 aa long. In addition, the complementarity in charge and shape of this chamber with the substrate also determines the substrate selectivity as exemplified by the insulin-bound IDE structure.[21] Apart from these unique properties of the IDE catalytic chamber, IDE also has a highly conserved exosite located approximately 30 Å away from the zinc ion bound at the catalytic center.[19] The structures of IDE in complex with Aβ, glucagon, insulin, and bradykinin reveal that this exosite serves as an anchoring site for the N-termini of IDE substrates.[3,20,21] Such an interaction is hypothesized to serve as a molecular ruler, directing IDE to perform the initial cleavage at least 10 aa away from the N-terminal end of its longer substrates.[1] In addition, the binding of the exosite with a shorter peptide substrate could reduce the apparent size of the catalytic chamber.[20] This is postulated to facilitate the cleavage of short substrates of IDE such as 9-aa-long bradykinin. However, it remains unclear how IDE utilizes the properties of the catalytic chamber and exosite to recognize and selectively degrade substrates such as IGF-II, TGF-α, and amylin.

IDE exhibits preferential cleavage of the structurally related IGF and epidermal growth factor (EGF) proteins, peptide hormones that contain three disulfide bonds each.[1,15–17,22] IGF-I and IGF-II are structurally and functionally related to insulin.[23,24] Together with insulin, this IGF family is involved in regulation of multiple biological processes including carbohydrate metabolism, growth, life span, development, and neoplasia.[25,26] NMR analysis reveals that the structure of IGF-II is similar to that of insulin and IGF-I.[23] Similar to insulin, IGF-II is also a high-affinity (~100 nM) substrate of IDE and is rapidly degraded by this enzyme.[1] Paradoxically, IDE binds IGF-I with reduced affinity compared to IGF-II and does not effectively degrade this hormone. EGF and TGF-α are structurally related growth factors that work in the endocrine, paracrine, and autocrine systems for various biological activities.[27–29] Similar to the IGF family, IDE also selectively degrades TGF-α over EGF.[17] The sites where IDE cleaves IGF-II and TGF-α are mostly unknown, as is the molecular basis of substrate selectivity among members within the IGF family and the EGF family.

IDE prefers to degrade amyloidogenic peptides such as amylin, or islet amyloid polypeptide,[13] a 37-aa peptide containing a disulfide bond near the N-terminus, between cysteine 2 and cysteine 7. Amylin is normally produced by pancreatic β cells along with insulin to control glucose homeostasis.[30] Similar to Aβ, amylin can induce cell death of pancreatic β cells and may thus be involved in the development of diabetes.[30,31] We have previously identified the cleavage sites of amylin by IDE, as well as solved the structure of human IDE in complex with amylin in the presence of a reducing agent.[3] The reducing agent was required for the crystallization of human IDE protein. However, since a reduced environment breaks disulfide bonds, the molecular basis for the interaction of IDE with amylin that retains the disulfide bond remains elusive.

Fig. 1. Characterization of the degradation of IGF-II and TGF-α by IDE. (a) Primary sequences of human IGF-II, TGF-α, and insulin. Disulfide bonds are shown by a line connecting two cysteines. Arrows on IGF-II and TGF-α depict the cleavage sites by IDE from this analysis while the cleavage sites of insulin are as reported previously.[21] The underlined amino acids are observed in the crystal structures of substrate-bound IDE. (b) Comparison of secondary structure (left) and electrostatic surface representation (right) of IGF-II, TGF-α, and insulin. PDB accession codes of IGF-II, TGF-α, and insulin are 1IGL, 1YUF, and 1G7A, respectively. The molecular surface is colored as calculated by APBS[32] (<−6 kT in red, 0 kT in white, and >+6 kT in blue). (c) Inhibition of the IDE-mediated degradation of the fluorogenic substrate V (a bradykinin-mimetic) by insulin, TGF-α, and IGF-II. IDE (1 μg) was mixed with substrate V (450 nM) in the presence of indicated concentrations of insulin, TGF-α, and IGF-II, and fluorescence intensity was monitored for 10 min at 37 °C. Results (means±SD) are representative of three independent experiments performed in duplicate. (d) and (e) show the representative MS/MS spectrum for N-terminal regions of IGF-II and TGF-α, respectively. The ESI-tandem mass spectrum of the 529.229 ion from IDE-digested TGF-α at m/z 1584.668 (left) and the 976.469 ion from IDE-digested IGF-II at m/z 1950.936 (right). The amino acid sequence and ion identification of the tandem mass spectrum are shown, and experimentally observed ions are labeled in the sequence.

IDE's ability to degrade a wide variety of substrates that differ in length, structure, and biological properties is of great interest in the fields of diabetes and Alzheimer's research. Determining the mechanism of how IDE recognizes and degrades certain substrates over others as well as how it degrades amyloidogenic peptides is a crucial step in understanding how IDE affects the homeostasis of these peptides in the human body. In order to understand how IDE differentiates and degrades IGF-II, TGF-α, and amylin without breaking their disulfide bonds, we performed structural and biochemical studies on these IDE substrates. We took advantage of the high-accuracy mass spectrometry (MS) to identify the products of IGF-II, TGF-α, and amylin digestion by IDE. To eliminate the need for a reducing agent

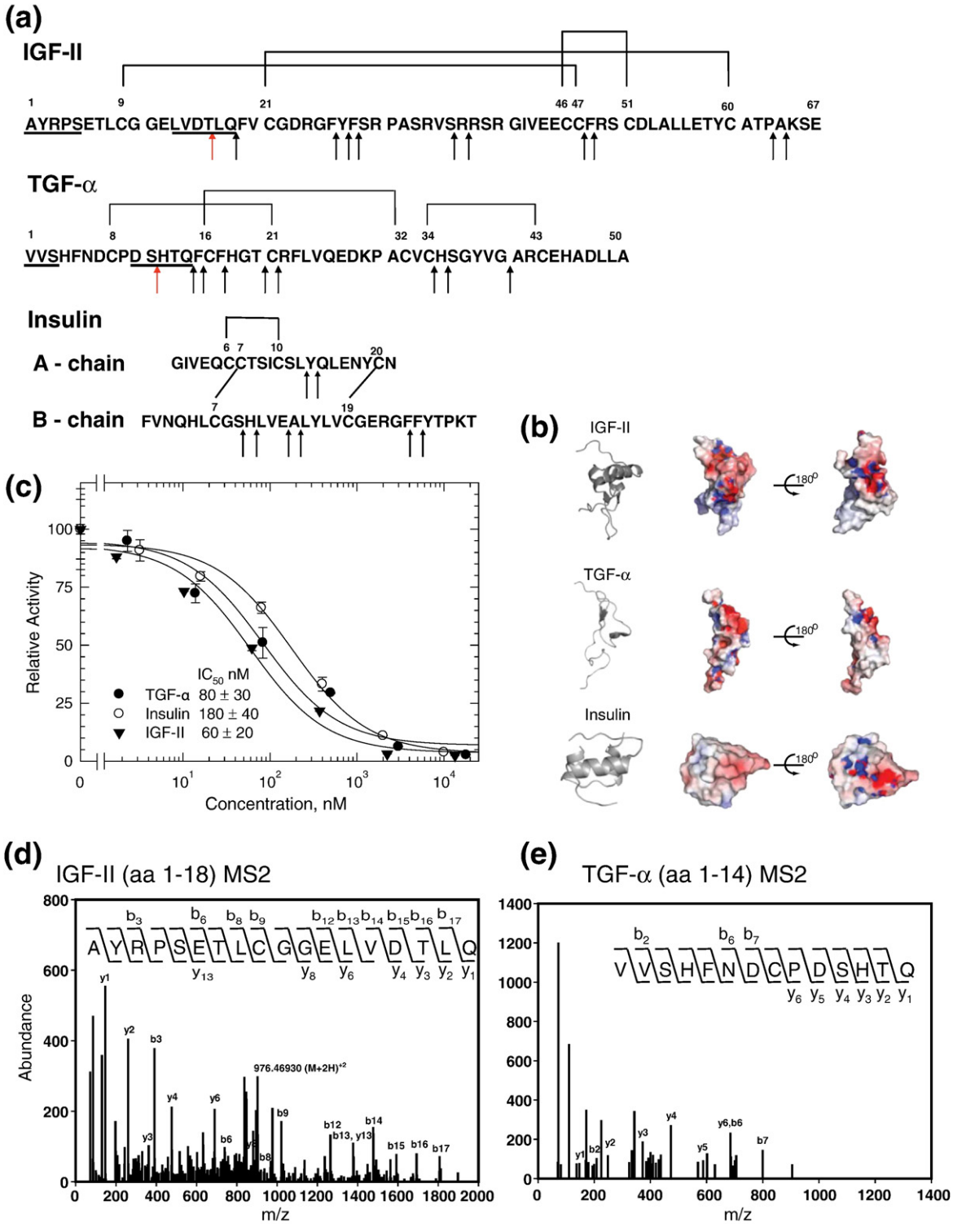

Fig. 1 (*legend on previous page*)

during the crystallization of IDE, we mutated all 13 cysteines in human IDE to construct a fully functional, cysteine-free IDE.[20,21] Using this construct, we determined the structures of human IDE in complex with three disulfide-containing substrates: IGF-II, TGF-α, and amylin. Together with the NMR structures of these three substrates and other peptides within the same families, new insights regarding how IDE uses its exosite and catalytic chamber to bind, unfold, and degrade these disulfide bond-containing substrates emerge.

Results

Mass spectroscopy analysis of the degradation of IGF-II and TGF-α by IDE

IGF-II is a 67-aa growth-promoting hormone that plays a vital role in embryo development and epigenetic imprinting. TGF-α is a 50-aa-long peptide that can induce epithelial cell development. These two peptides differ significantly in their primary sequences, secondary structure, shape, and surface charge distribution (Fig. 1a and b).[33–35] However, like insulin, these two peptides are high-potency inhibitors (60–180 nM, Fig. 1c) for the degradation of a fluorogenic bradykinin-mimetic peptide, substrate V by human IDE. The IC_{50} values are in agreement with the reported K_i values.[4,16,17,22] Thus, IDE binds IGF-II and TGF-α, two structurally diverse disulfide-bond-containing peptides, with high affinity comparable to that of insulin.

IDE can effectively cleave both IGF-II and TGF-α but little is known regarding cleavage sites for each substrate. Both IGF-II and TGF-α are stabilized by three intramolecular disulfide bonds. IDE is known to degrade its substrates without the assistance of disulfide bond isomerase activity, and its proteolytic activity does not require the breakage of any disulfide bonds. To decipher the cleavage sites of IGF-II and TGF-α, we used liquid chromatography coupled with quadruple time-of-flight (LC-Q-TOF) MS. We identified 14 IGF-II fragments and 8 TGF-α fragments that were generated by 5-min incubations with IDE followed by treatment with a reducing agent, DTT (Table 1). The identification of these fragments is based on the accurate match of the observed mass with the predicted mass of the precursor and b/y product ions. Figure 1d and e show sample mass spectra obtained for IGF-II and TGF-α, respectively. We also performed matrix-assisted laser desorption/ionization (MALDI)-TOF tandem MS to gain better MS/MS coverage of these precursor ions and confirm the identity of these fragments (Table S1).

Similar to the cleavage pattern of insulin by IDE, we found that IDE preferentially cleaves several discrete regions of IGF-II and TGF-α (Fig. 1a). Several of these sites are clustered together. These include three pairs of cleavage sites on IGF-II, amino acids 36–37/37–38, amino acids 47–48/48–49, and amino acids 63–64/64–65, and three pairs of cut sites on TGF-α, amino acids 14–15/15–16, amino acids 20–21/21–22, and amino acids 34–35/35–36. In one case, we also observed three cleavage sites that are adjacent to each other (amino acids 26–27, 27–28, and 28–29) on IGF-II. This is consistent with the probabilistic mode of binding of these regions to the catalytic cleft for cleavage. Such biased stochastic mode is a commonly found feature of IDE substrate cleavage sites.[1,3,4,21] We did not observe cleavages near the N-terminus of either IGF-II or TGF-α (Fig. 1a). This is consistent with the notion that IDE uses the exosite to anchor the N-termini of both substrates; thus, no cleavage can occur at the first 10 aa residues of the N-terminal end. Interestingly, the cleavage sites of TGF-α defined using the accurate mass determination differ significantly from those determined by the blockage of Edman degradation of rat IDE-degraded [^{125}I]TGF-α.[36] Such a discrepancy may be due to the methodology and/or source of IDE.

Table 1. Summary of IDE-degraded fragments of IGF-II and TGF-α

	Observed (M+H)	Calculated (M+H)	Δppm
IGF-II			
1–16	1709.796	1709.793	1.67
1–18	1950.936	1950.935	0.42
17–26	1140.543	1140.539	3.64
17–27	1303.602	1303.603	0.51
17–28	1450.670	1450.675	3.49
19–28	1209.528	1209.533	1.65
37–48	1453.692	1453.690	1.28
37–67	3505.657	3505.659	0.57
38–48	1297.590	1297.591	0.19
38–67	3349.556	3349.573	5.07
49–63	1654.769	1654.770	0.11
49–64	1725.807	1725.809	1.40
48–67	2217.045	2217.052	3.36
49–67	2069.976	2069.980	2.13
TGF-α			
1–11	1218.497	1218.498	0.53
1–14	1584.663	1584.668	3.64
1–15	1731.731	1731.738	4.04
1–17	1981.809	1981.811	0.94
12–21	1179.459	1179.458	0.85
35–50	1697.794	1697.795	0.59
36–50	1560.735	1560.739	2.56
41–50	1097.529	1097.534	4.56

Assignment of the most prominent peaks generated after 5-min incubation with IDE using Q-TOF MS/MS.

MS analysis of the degradation of amylin and Aβ(1–40) by IDE

Previously, we used MALDI-TOF MS to assess the cleavage sites of amylin and Aβ(1–40) by IDE.[3] To more accurately determine the cleavage sites, we used Fourier transform ion cyclotron resonance (FT-ICR) MS for its high mass accuracy and sensitivity (Table 2 and Table S2). Based on the excellent match of the precursor ions to the predicted mass as well as the extensive coverage of b and y product ions from each precursor ion, we identified seven major

Table 2. Ion identification of major IDE-degraded fragments of amylin and Aβ(1–40)

	Observed (M+H)	Calculated (M+H)	Δppm	Observed b/y ions[a]
Amylin[b]				
1–15 (C–C)[c]	1639.7677	1639.7873	13.2	b7–b13, y5–y6
16–27	1271.6722	1271.6936	16.9	b3–b5, b7–b11, y7–y9
16–28	1358.7054	1358.7257	14.9	b3, b5–b11, y6–y7, y9–y10
19–34	1554.7352	1154.7588	20.5	b4–b14, y6, y11–y13
23–34	1152.6000	1152.6089	7.7	b2–b11, y4–y10
23–36	1367.6867	1367.6995	9.3	b3–b6, b8–b13, y2–y11
Amylin[b] *(+TCEP)*				
16–27	1271.6741	1271.6936	15.3	b2–b5, b7–b11, y5, y7–y9
16–28	1358.7127	1358.7257	9.6	b3–b11, y6–y7, y11
16–37	2281.1128	2281.1207	3.5	b5, b7–b10, y5–y10, y12–y17
23–34	1152.6000	1152.6089	7.7	b3–b11, y6–y7, y9
23–36	1367.6866	1367.6995	9.4	b3–b13, y2–y11
Aβ(1–40)[d]				
19–40	2180.1456	2180.1420	1.6	b5–b6, b9, b11–b18, y6–y10, y16–18
21–40	1886.0096	1886.0052	2.3	b9–b17, y5–y9, y13, y16
20–40	2033.0727	2033. 0736	0.4	b9, b11–b17, y5–y10, y12–y14, y16–y17
1–28	3261.5354	3261.5328	0.8	b5–b8, b10–b13, y4–y6, y8–y13
15–40	2648.4593	2648.4480	4.3	b6, b8–b10, b17–b18, y7–y11, y13, y16–y18
14–40	2785.5235	2785.5069	6.0	b5–b12, b14–b15, b17–b18, y8–y10, y13, y16–y20

[a] The b and y product ions of the most prominent fragment peaks of IDE-degraded amylin, reduced amylin, and Aβ(1–40) are generated by LC-ESI-FT-ICR-MS-CID-MS/MS, and their identity is analyzed using MassMatrix webserver (http://searcher.rrc.uic.edu/cgi-bin/mm-cgi/search_form.py).
[b] Five-minute incubation of amylin with IDE in 50:1 ratio.
[c] This fragment has an intact disulfide bond.
[d] One- to five-second incubation of Aβ(1–40) with IDE.

cleavage sites when the non-reduced amylin was used (Table 2 and Fig. 2c). We also performed the cleavage reaction in the presence of a reducing agent, tris(2-carboxyethyl)phosphine (TCEP), to assess whether the presence of disulfide bond in amylin affects the cleavage site of amylin by IDE. While six out of seven amylin cleavage sites were also cut by IDE when amylin was reduced by TCEP, we did not observe the cleavage between residues 18 and 19, which is located in the middle of amylin (Table 2; Table S2; Fig. 2c). This indicates that the presence of disulfide bond can alter the cleavage site of amylin by IDE.

We have analyzed the initial cleavage sites of insulin by IDE to gain the mechanistic understanding of insulin degradation by IDE.[21] While IDE is known to cleave Aβ(1–40) at multiple sites, the preferred initial cleavage sites have not been defined yet.[3,37] To address this, we performed the digestion of Aβ(1–40) by IDE by varying the time of incubation and then assessed the cleavage products by FT-ICR MS/MS (Table 2). As expected, IDE cleaves Aβ(1–40) at multiple sites even only at brief incubation (1–5 s). Our MS analysis reveals the preferred initial cleavage sites of Aβ(1–40) by IDE to be in the middle of Aβ(1–40) (amino acids 18–19, 19–20, and 20–21). The cleavages at amino acids 14–15, amino acids 15–16, and amino acids 28–29 occurred less frequently (Table 2; Fig. 2c). These data are consistent with our proposed yet unproven model that, upon the anchoring of N-terminus of Aβ to the IDE exosite, the middle segment of Aβ is preferably cut in a probabilistic manner for its initial cleavage, which would prevent the amyloid fiber formation by Aβ.[1]

Structures of amylin-, Aβ(1–42)-, IGF-II-, and TGF-α-bound IDE

Previous structural studies of IDE with various substrates have required the use of a reducing agent in the crystallization conditions, due to the presence of 13 cysteine residues in human IDE.[3] This reduced environment also breaks any disulfide bond(s) in the substrates, resulting in IDE–substrate complexes that may not reflect the native enzyme–substrate binding conformation. We have recently constructed a catalytically inactive, cysteine-free IDE (IDE-CF-E111Q) that can be crystallized without the reducing agent.[1,21] Using this mutant, we re-examined the structural basis of the interactions of IDE with amylin, a substrate containing one disulfide bond. We have solved the crystal structure of IDE-CF-E111Q in complex with amylin at 2.9 Å resolution (Fig. 2a; Table 2). While we were unable to observe the disulfide bond in the previous IDE–amylin structure,[3] the current structure shows a density that fits well with residues K1–N3, C7–A8, and L12–L16, with a disulfide bond present between C2 and C7 (Fig. 2b). However, we could not see density for the majority of the loop formed by amino acids 4–6 of amylin. Thus, we do observe two discreet segments of amylin, an N-terminal portion in the exosite and another segment in catalytic site of the enzyme; this spatial separation of the substrate is a common feature in IDE–substrate structures. It is worth noting that, similar to the structures of previous IDE–substrate complex, the averaged thermal *B*-factors of the amylin is higher than that of IDE (Table 3).[3,21] This is presumably due to the structural heterogeneity of the substrates and/or less than 100%

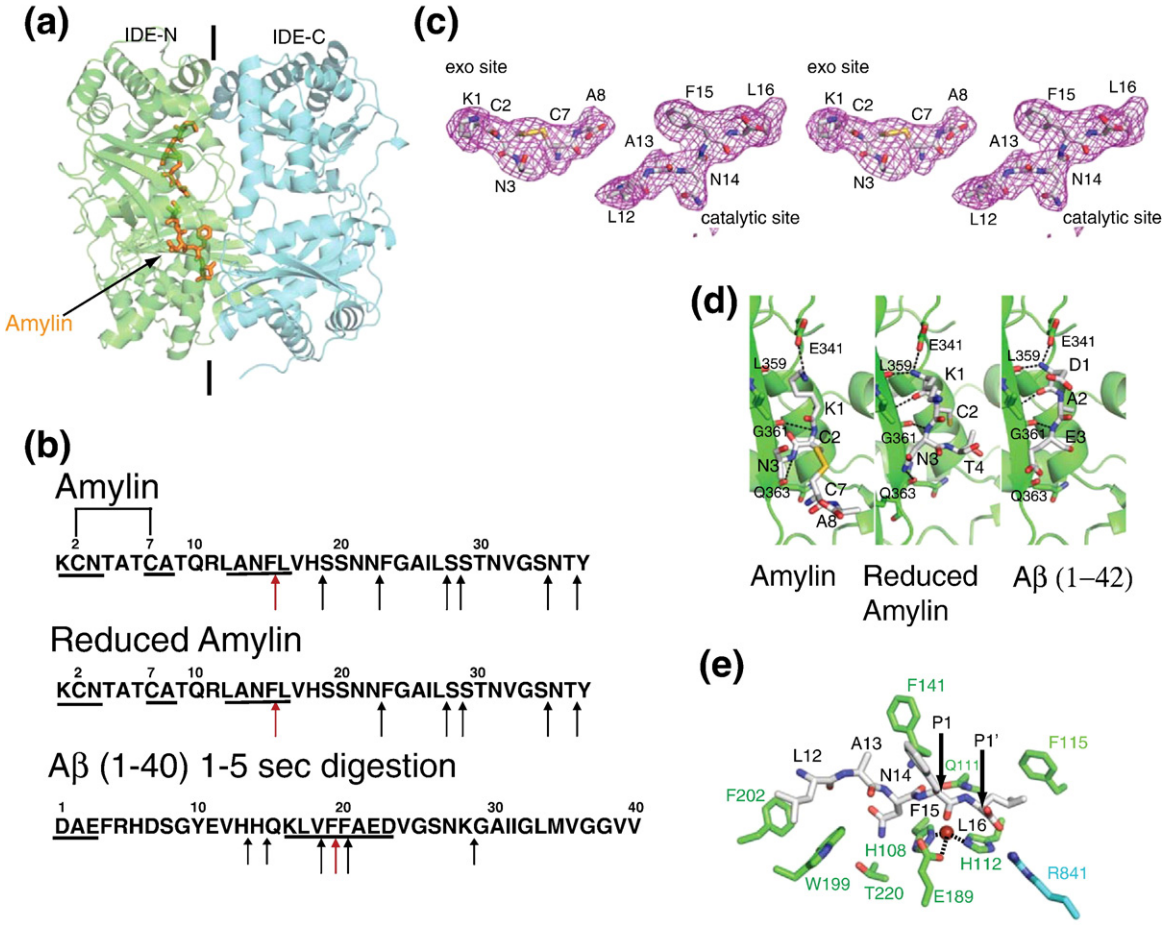

Fig. 2. Structures of IDE in complex with amylin. (a) Global view of the structure of amylin-bound IDECF-E111Q monomer. IDE-N and IDE-C are colored green and cyan, respectively. Amylin is in the stick representation colored orange. (b) Stereo view of composite omit map (purple) of the IDE-bound amylin is contoured at 1.5 σ. Oxygen, nitrogen, and carbon atoms of amylin are shown in red, blue, and orange, respectively. (c) Primary sequences of amylin, reduced amylin, and Aβ(1–40). The arrows on the amylin depict the cleavage sites by IDE as experimented and the arrows on Aβ(1–40) depict the cleavage sites by IDE after short (1–5 s) incubation. The minor cleavage sites on Aβ(1–40) are marked with the shorter arrows. The underlined amino acids with the scissor bond marked by a red arrow are observed in the crystal structures of substrate-bound IDE. (d) Detailed interaction of the N-terminus of non-reduced amylin (left), reduced amylin (middle), and Aβ(1–42) (right) with the exosite of IDE. (e) Detailed interaction of amylin with the IDE catalytic site. The color of IDE residues corresponds to the respective color of IDE domain in (a). The PDB codes for structures of amylin-bound IDE-CF-E111Q, reduced amylin-bound IDE-E111Q, and Aβ(1–42)-bound IDE-CF-E111Q are 3HGZ, 2G48, and 2WK3, respectively.

occupancy (despite the extensive effort in loading amylin to IDE in order to ensure the high occupancy, see Methods). The same phenomenon was observed in the structures of IDE bound to Aβ(1–42), IGF-II, and TGF-α described below (Table 3).

Amylin and Aβ, another IDE substrate, are both amyloidogenic peptides and both can be effectively cleaved at multiple locations (Fig. 2c). The structure of Aβ(1–40) in complex with IDE has previously been solved, as have the cleavage sites for amylin and Aβ by IDE.[3] Aβ(1–42) is a form of Aβ that forms amyloid plaque much faster than Aβ(1–40) and serves as a better marker for the progression of Alzheimer's disease. To learn whether IDE recognizes these two peptides differently, we also solved the structure of IDE in complex with Aβ(1–42) (Table 2). We found the binding of Aβ(1–42) to the exosite and catalytic site of IDE in this structure to be virtually identical with that of Aβ(1–40) in our Aβ(1–40)-bound IDE structure. Compared to the Aβ-bound IDE structure, we found a novel interaction of amylin with the exosite of IDE (Fig. 2d). The disulfide bond formed by amylin C2 and C7 changes the local hydrogen bond network to the IDE β12-strand compared to Aβ (Fig. 2d). Most noticeably, the side chain of the N-terminus of amylin (K1) forms a salt bridge with that of IDE E341. This is different from other substrates of IDE, where the amino-terminus of the substrates (i.e., Aβ) forms hydrogen bonds with the side chain of E341 and the main chain of L359.

The structure of amylin at the catalytic site of IDE shows that amylin is embedded into several hydrophobic pockets, and amylin residues F15 and

L16, positioned nearby the catalytic metal ion, are coordinated by H108, H112, and E189 of IDE (Fig. 2e). These hydrophobic interactions include the contacts of amylin L12 with IDE F202 and W199, that of amylin F15 with IDE F141, and that of amylin L16 with IDE F115. This corresponds to the biochemical data available for amylin, which indicate that the cleavage between residues 15 and 16 is indeed one of the major cleavage sites (Fig. 2c and e).[3]

The crystal structures of IDE-CF-E111Q complexed with IGF-II and TGF-α were determined at 2.3 Å resolution to further understand how IDE binds different substrates (Table 2). The overall fold of IDE in both cases is nearly identical with amylin-bound IDE (Fig. 3a), with two discrete substrate segments clearly visible: one at the exosite and the other at the catalytic site of the respective structures (Fig. 3b). Both main chains and side chains of the first 5 aa of IGF-II are visible, while only the main chains of the first 3 aa of TGF-α are visible (Fig. 3c). At the catalytic site, several residues of IDE located in domains 1 and 4 form a largely polar cavity with hydrophobic patches that interact with cleavage sites in both substrates (Fig. 3d). At the catalytic site of IDE, IGF-II amino acids 13–18 and TGF-α amino acids 10–14 fit nicely into the electron density map, and the observed primary cleavage sites of these two substrates (T16–L17 of IGF-II and S11–H12 of TGF-α) appear poised for cleavage (Fig. 3d).

Discussion

IDE cleaves multiple substrates that have various biological functions, including amylin, Aβ, IGF-II, and TGF-α. These substrates are diverse in their sequence, size, and structure. Based on accumulated structural and biochemical evidence, it has been proposed that the catalytic cycle and substrate specificity of IDE revolve around a conformational switch between the open and closed states of this enzyme, with interactions between potential substrates and the IDE catalytic chamber stabilized by complementary electrostatic properties (Fig. 4).[1,3] We propose that IDE normally exists in an equilibrium between an open (IDE^O) and a closed (IDE^C) state.[3] In the open state, the negatively charged interior of the IDE-N domain and the positively

Table 3. Data collection and structure refinement statistics of substrate-bound IDE

	IDE–IGF-II	IDE–TGF-α	IDE–amylin	IDE-Aβ(1–42)[a]
Data collection				
Beamline	APS 19ID	APS 19ID	APS 19ID	APS 19ID
Space group	$P6_5$	$P6_5$	$P6_5$	$P6_5$
Cell dimension (Å)				
a	263.0	262.2	262.9	261.6
b	263.0	262.2	262.9	261.6
c	90.8	90.5	90.9	90.7
Resolution (Å)	50–2.28	50–2.3	50–2.9	50–2.6
R_{sym} (%)[b]	13.4 (50.7)	9.4 (52.0)	8.0 (33.2)	9.1 (45.3)
I/σ	20.5 (2.1)	23.6 (3.6)	25.1 (3.8)	17.6 (3.0)
Redundancy[c]	5.4 (3.1)	7.1 (6.8)	5.7 (4.3)	3.6 (3.4)
Completeness (%)	99.7 (96.9)	99.8 (100.0)	99.9 (99.2)	99.8 (99.9)
Unique reflections	162,414	157,230	79,043	109,059
Refinement				
R_{work}[d]	0.206	0.191	0.178	0.186
R_{free}[e]	0.239	0.231	0.223	0.232
No. of atoms				
Protein	15,710	15,644	15,818	15,590
Water	598	653	346	233
B-factors				
IDE	35.5	28.6	38.6	35.2
Substrate	54.2	52.6	67.8	71.2
Water	44.5	46.5	48.5	36.5
r.m.s.d.				
Bond lengths (Å)	0.015	0.016	0.012	0.022
Bond angles (°)	1.363	1.463	1.406	1.959
Ramachandran plot (%)[f]				
Favorable region	91.9/91.6	92.3/91.2	89.6/90.0	90.7/100.0
Allowed region	8.1/8.4	7.3/8.8	10.4/10.0	9.3/0.0
Generously allowed region	0/0	0/0	0/0	0/0
Disallowed region	0/0	0/0	0/0	0/0
PDB code	3E4Z	3E50	3HGZ	2WK3

The outer resolution shell. Values in parentheses indicate the highest-resolution shell.

[a] The backbone nitrogen of Gly29 of Aβ(1–42) is substituted with 2-nitrobenzyl group to improve the solubility of Aβ(1–42) (Erik Johnson, University of Chicago, PhD thesis).

[b] $R_{merge} = \sum(I - \langle I \rangle)/\sum\langle I \rangle$.

[c] N_{obs}/N_{unique}.

[d] $R_{work} = \sum_{hkl} | \, | F_o | - k | F_c | \, | / \sum_{hkl} | F_o |$.

[e] R_{free}, calculated the same as for R_{work} but on the 5% data excluded from the refinement calculation.

[f] Values for IDE protein/substrate.

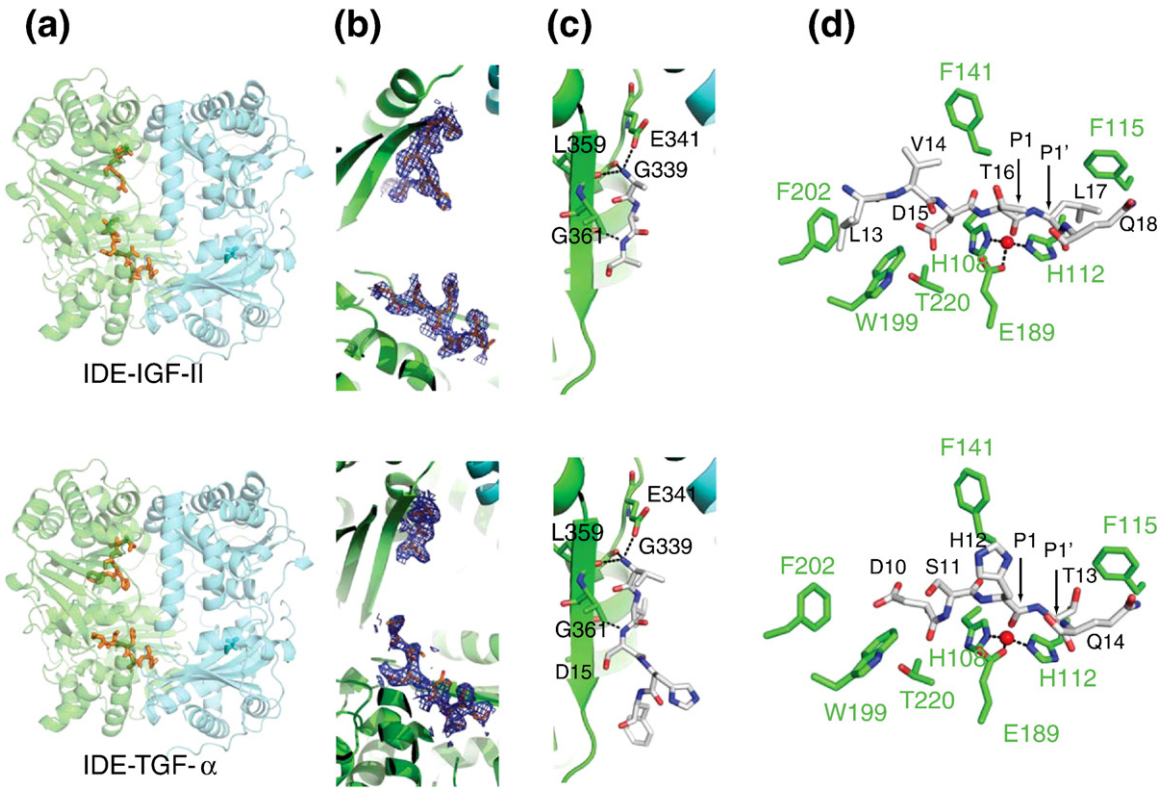

Fig. 3. Structures of IDE in complex with IGF-II and TGF-α. (a) Global view of the structure of IGF-II-bound (top) and TGF-α-bound (bottom) IDE-CF-E111Q monomer. IDE-N and IDE-C are colored green and cyan as Fig. 1. IGF-II and TGF-α are colored orange. (b) Composite omit maps (blue) of IGF-II and TGF-α are contoured at 1.5 σ. The substrates are colored orange. (c) The detailed interaction of the N-terminus of IGF-II and TGF-α with the exosite site of IDE. (d) Detailed interaction of IDE catalytic chamber with IGF-II and TGF-α. Oxygen, nitrogen, and carbon atoms of substrates are shown in red, blue, and orange, respectively.

charged interior of the IDE-C domain result in selective binding of ligands with charge distributions complementary to the electrostatic properties of the chamber (Fig. 4a). IDE substrates IGF-II, TGF-α, and amylin also exhibit such a charge distribution (Fig. 4b). Modeling the N-terminal end of IGF-II, TGF-α, or amylin in the exosite of IDE reveals charge complementarity between the substrate and the IDE chamber, as the negatively charged surfaces of IGF-II, TGF-α, and amylin fit well with the positively charged chamber wall of IDE-C.

The interactions between the substrate and the IDE chamber would appropriately position the flexible N-terminus of the substrate to bind at the exosite (Fig. 4a). The binding of the substrate N-terminus to the IDE exosite and/or the charge complementarity of the catalytic chamber of IDE with the substrate would facilitate the switch of the open conformation to the closed conformation, which is the preferred state of IDE.[1,3] By comparing the native NMR structures of IGF-II, TGF-α, and amylin with those in the IDE-bound structures, we find that IDE binding also results in a substantial substrate conformational change (Fig. 4c and d). The native conformation of the substrates does not position the putative cleavage sites close enough to the zinc-coordinated catalytic center of IDE, suggesting that a change in secondary structure must occur prior to catalysis. For three peptides, the most noticeable change was the conversion of IGF-II amino acids 13–18, TGF-α amino acids 10–14, and amylin amino acids 16–23 from α-helices to β-strands. These required conformational changes for IGF-II, TGF-α, and amylin are similar to those found in IDE in complex with Aβ and glucagons.[3] In addition, while IGF-II and amylin fit well in the catalytic cavity, the native conformation of TGF-α has an elongated shape and would extend beyond the walls of the chamber, potentially interfering with the switch from IDE^O to IDE^C (Fig. 4b). Since IDE does cleave TGF-α, this offers further evidence that an induced-fit structural rearrangement of substrates would be required for binding and cleavage within the catalytic chamber of IDE. While speculative, structural rearrangement of the substrate, at least in some cases, must occur prior to the formation of IDE^C.

The structural rearrangement would allow certain sections of IDE substrates to fit into the catalytic cleft of IDE for cleavage in a biased stochastic manner. This is consistent with the multiple cleavage sites found by our MS analysis on the degradation products of IGF-II, TGF-α, and amylin as well as the previous analysis of cleavage sites and products of IDE substrates. With the anchoring

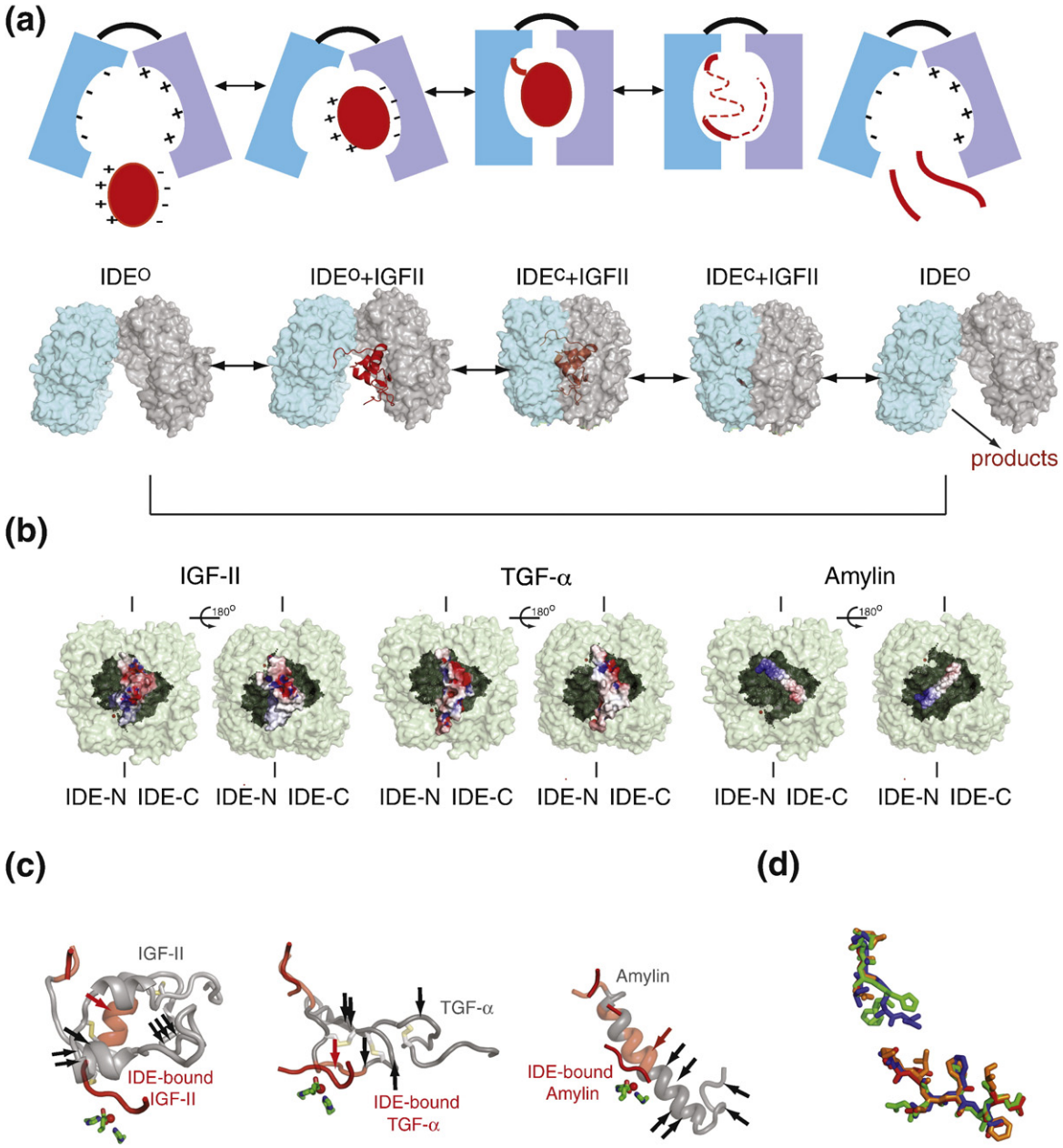

Fig. 4. Analysis of IDE's binding with IGF-II, TGF-α, and amylin. (a) A model of how IDE binds, unfolds, and degrades its substrate. IDE has two conformational states: the open state, IDE^O, and the closed state, IDE^C. The IDE-N and IDE-C are depicted as green and cyan, respectively. IGF-II (PDB code: 1IGL) is depicted as red cartoon. IDE^O is theoretically modeled based on the substrate free *E. coli* pitrilysin structure (1Q21); IDE^C corresponds to the atomic coordinate of IDE-CF-E111Q-IGFII (3E4Z). The detailed description of the mechanism is in Discussion. (b) Shape and surface charge distribution of IGF-II (left), TGF-α (middle), and amylin (right) modeled in the catalytic chamber of IDE. (c) Comparison of IGF-II (left), TGF-α (middle), and amylin (right) in their free forms (transparent gray) with IDE-bound forms (red). The segments in the free forms of IGF-II and TGF-α corresponding to IDE-bound forms are colored transparent red. The arrows indicate the cleavage sites, and the disulfide bonds are colored yellow. (d) Comparison of IDE-bound IGF-II (red), TGF-α (green), amylin (blue), and Aβ(1–42) (orange) in stick model.

of the N-terminus of substrates to the exosite that is 30 Å away from the catalytic center, the given section would likely to be at least 10 residues away from its N-terminus for the initial cleavage. Indeed, we found that the preferred initial cleavages of Aβ(1–40) occur in the middle of the peptide (amino acids 18–21). In addition, this anchor-dependent cleavage could also explain our structural and MS observations that the presence of a disulfide bond in amylin could constrain and alter the binding of amylin to the catalytic chamber of IDE so that an additional cleavage site between residues 18 and 19 of amylin can be cut. The initial cleavage can induce further conformational changes in the substrate, allowing for further cleavage inside the catalytic chamber. Such processive cleavages for the initial

digestion of insulin allows IDE to cut it into two pieces and inactivate its function without breaking the disulfide bonds of insulin.[21] Ultimately, the cleavage could induce IDE to switch to the open conformation, leading to release of the proteolytic fragments and allowing for incorporation of other substrates or intermediate degraded fragments to start a new degradation cycle.

Our structures, together with the secondary structures and amino acid composition of the IGF and EGF family hormones, reveal that charge complementarity and exosite anchoring are used by IDE to selectively degrade certain members of those hormone families. IGF-II and IGF-I share 64% sequence identity while TGF-α and EGF share 36% sequence identity (Fig. 5a). Accordingly, their structures are highly homologous within each family (Fig. 5b). The r.m.s.d. of TGF/EGF is 2.536 Å, while that of IGF-I/IGF-II is 1.298 Å. However, the surface charge distributions between peptides in the same family differ. TGF-α has a much higher dipole moment (200 Debyes) than that of EGF (90 Debyes) and, compared to EGF, has a better charge complementarity for the catalytic chamber of IDE (Fig. 5b). IGF-II has a clear dipole charge distribution (330 Debyes) that could complement the charged catalytic chamber of IDE (Fig. 5b).[38] On the other hand, despite having only a slightly lower dipole moment than IGF-II (300 Debyes, Fig. 5c), the surface charge distribution of IGF-I does not coordinate well with the IDE chamber. Thus, within this growth family, the dipole moment and charge complementarity could be used as the parameters to predict susceptibility to IDE.

Currently, the role played by the specific substrate sequences in determining IDE selectivity is unclear. However, it is worth noting that IGF-I residues R55 and R56 would form a positively charged region that would contact the positively charged chamber of IDE-C, decreasing the binding affinity of IGF-I. The corresponding residues in IGF-II, A55 and L56, are nonpolar. The same situation can be observed from the comparison of TGF-α and EGF. EGF contains positively charged R45 and R48, which

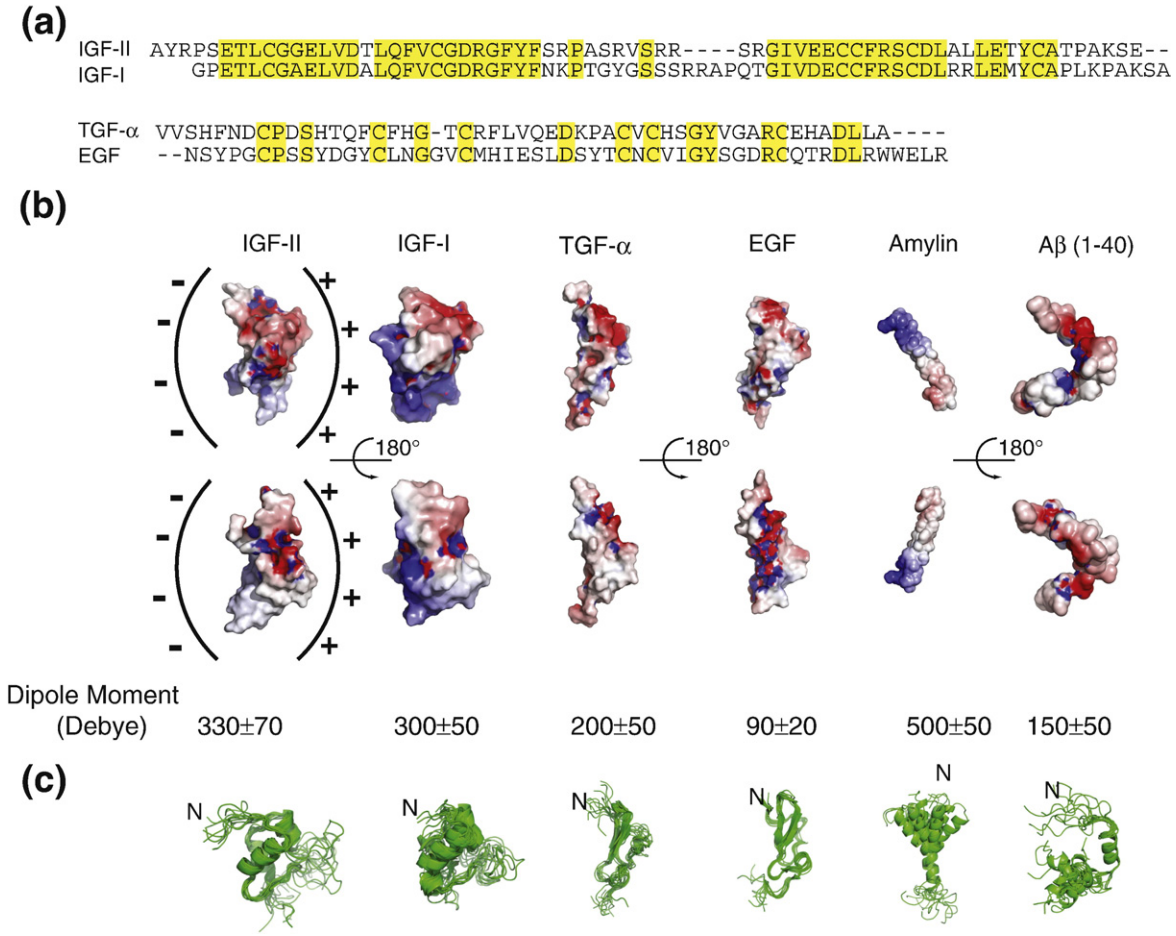

Fig. 5. Structural comparison of IGF, EGF, and amyloidogenic peptides. (a) Sequence alignment of the IGF-II/IGF-I and TGF-α/EGF. (b) Comparison of the electrostatic surface of IGF-II (1IGL), IGF-I (3GF1), TGF-α (1YUF), EGF (1EPH), amylin (2KB8), and Aβ(1–40) (1AML). The molecular surface is colored as calculated by APBS[32] (<−6 kT in red, 0 kT in white, and >+6 kT in blue). The dipole moment of these peptides was the average from distinct NMR solution structures [10 for IGF-I, 20 for IGF-II, 16 for TGF-α, 10 for EGF, 20 for Aβ(1–40), and 30 for amylin].[38] (c) NMR solution structures of IGF-II, IGF-I, TGF-α, EGF, amylin, and Aβ(1–40).

would contact IDE-C and can interfere with the first step in IDE–substrate binding as outlined in our model.

Amylin and Aβ are both amyloidogenic peptides, exhibit bipolar surface charge distributions, and share 36% sequence similarity. Comparison of NMR structures of these peptides reveals that amylin has a high dipole moment (500 Debyes), allowing it to complement well with the charge distribution of the catalytic chamber of IDE (Fig. 5b and c). However, such charge complementarity is not observed for Aβ. Furthermore, these two peptides are much smaller compared to the IGF and EGF family peptides that they are likely to have more flexibility in their interaction with the IDE chamber. Thus, it is difficult to assess the relative contribution of charge distribution and conformational flexibility for the binding and degradation of Aβ and amylin by IDE.

A common feature between the amylin-, IGF-II-, and TGF-α-bound IDE structures is the interaction of the substrate's N-terminus with the IDE exosite. Indeed, this feature has also been observed in our previously reported IDE–substrate structures, indicating that this is an important interaction for IDE–substrate binding. In comparing the NMR structures of IGF-II and IGF-I, we see that both have a relatively stable helix domain in the middle, while the conformations of the N- and C-termini vary greatly (Fig. 5c). A significant difference can be seen at the N-terminus of IGF-II, which is longer and more flexible than that of IGF-I. A longer and more flexible N-terminus can also be observed for TGF-α compared to EGF and Aβ compared to amylin. We hypothesize that a longer and more flexible N-terminus increases the possibility that the substrate will make the appropriate contacts for anchoring to the IDE exosite. In addition to the charge repulsion from the positive patches found in IGF-I and EGF, the failure of the N-termini of these growth factors to reach the exosite of IDE would also help to explain why IDE preferentially degrades IGF-II over IGF-I and TGF-α over EGF. Differences in the N-terminus may also explain why Aβ has a higher binding affinity than amylin. However, their structural dissimilarity and the bulkiness of the loop formed by the disulfide bond of amylin may also play a role in determining binding affinity.

Our biochemical assays and structures expand the repertoire of substrates that IDE is known to degrade and our knowledge of the IDE–substrate binding mechanism. Our comparative analyses of the IGF and EGF hormone families revealed that charge distribution and flexibility of the substrate N-terminus are important factors in IDE–substrate recognition and cleavage. Furthermore, proper placement of substrates in relation to the IDE catalytic site requires the requisite structural change of the substrates. Additional work, such as mutagenesis studies and N-terminal truncation/elongation, will be needed to verify our hypotheses. However, this study provides key information for the engineering of substrates with altered binding affinities to IDE for therapeutic applications.

Methods

Protein expression and purification

The expression vectors for cysteine-free human IDE (IDE-CF; C110L, C171S, C178A, C257V, C414L, C573N, C590S, C789S, C812A, C819A, C904S, C966N, and C974A) and the catalytically inactive IDE-CF-E111Q mutants were created as described previously.[21] Wild-type human IDE and IDE mutants were expressed in *Escherichia coli* Rosetta (DE3) cells (at 25 °C and 19 h, IPTG induction) and purified by Ni-NTA, Source-Q, and Superdex S-200 columns as described previously.[21] Insulin was purchased from RayBiotech, IGF-II and TGF-α were from Peprotech, and amylin amide was from Bachem.

MS analysis for TGF-α and IGF-II

Enzyme reactions were carried out at 37 °C by mixing 5 μl of 1 mg/ml TGF-α and IGF-II in 20 mM Hepes buffer (pH 7.2) with 5 μl IDE protein in an enzyme-to-substrate molar ratio of 1:50. Reactions were stopped by the addition of 30 μl stop solution (170 mM ethylenediaminetetraacetic acid and 0.07% trifluoroacetic acid). For MALDI-TOF MS, mass spectra were obtained in either linear or positive reflector mode using a Voyager 4700 MALDI-TOF mass spectrometer (Applied Biosystems).

For Q-TOF-MS2, a 0.3-μl aliquot of IDE-digested IGF-II and TGF-α was first incubated with 300 mM DTT for 30 min and then injected onto an Agilent 1100 LC system attached to an Agilent 6520 Q-TOF-MS equipped with a Chip-Cube nanoflow interface. A chip packed with Zorbax C18SB (75 μm internal diameter × 43 mm length, Agilent Technologies G4240-62001) was used to trap and elute the peptides, which were run using a gradient as follows: 0.1% formic acid in water is held at 100% for 5 min and then changed to 45% of a 10:90 mix of 0.1% formic acid in water:acetonitrile over 20 min and then changed to 75% of this mix over 10 min. The flow rate of the chromatography segment of the chip is 200 nl/min and that of the enrichment (trapping) segment is 3 μl/min. Enrichment is conducted for 5 min at 100% 0.1% formic acid in water. The Q-TOF-MS is run with the following parameters: MS1 scan range, 300–2000 m/z; MS/MS scan range, 50–3000 m/z; MS1 scan rate, 8.4 scans/s; MS/MS scan rate, 2 scans/s. Positive ion mode was used throughout the run with a source V_{cap} of −1875 V, a fragmentor voltage of 175 V, a drying gas temperature of 325 °C, and a gas flow rate of 5 L/min. For MS/MS, an isolation width of 4 amu was used to filter selected precursor ions into the collision cell, which had a ramped collision energy using a slope of 3 V/100 amu and an offset of 2 V. All data were collected as centroided to conserve disk space, and a reference compound simultaneously infused into the spray chamber with an m/z of 1221.99 was used to automatically recalibrate each spectrum as it was recorded.

The data acquired this way were subsequently qualitatively analyzed by using the molecular feature extractor tool built into the MassHunter (Agilent Technologies version B.03), resulting in the detection of all chromatographed peptides listed by monoisotopic mass. The results of these extractions were exported to Microsoft Excel. Masses detected were compared with lists of possible peptides derived from subsequences of the original protein subject to a minimum mass agreement of 5 ppm between detected peptides and predicted peptides.

MS analysis for amylin and reduced amylin

Enzyme reactions were carried out at 37 °C by mixing 5 μl of 1 mg/ml amylin in 20 mM Hepes buffer (pH 7.2) with 5 μl IDE protein in an enzyme-to-substrate molar ratio of 1:50 with or without 10 mM TCEP added. Reactions were stopped after 5-min incubation by the addition of 30 μl stop solution (170 mM ethylenediaminetetraacetic acid and 0.07% trifluoroacetic acid). The digested samples were then analyzed using FT-ICR MS. To do so, we injected amylin samples (12 μl) into a nano RP-HPLC system (Dionex), with a C18 analytical column (Agilent). Peptides were eluted from the nano column with a linear gradient of 5–95% acetonitrile in 0.1% formic acid and sprayed into an LTQ-FT tandem MS instrument (Thermo Scientific). Spectra were acquired using positive ion nano ESI mode with the FT-ICR acquiring precursor spectra from 200 to 2000 m/z. For tandem MS, precursor ions were fragmented by collision-induced dissociation. MS/MS spectra were acquired in a data-dependent manner from the five most intense precursor ions of each FT-ICR MS scan. The RAW data files are processed by Xtract™ function in Xcalibur™ (Thermo Fisher Scientific) to generate reduced data files containing the deconvoluted masses and intensities for MS spectra.

Protein crystallization and structure determination

IDE-CF-E111Q in complex with IGF-II, TGF-α, amylin, or Aβ(1–42) was made after five cycles of protein–substrate complex formation and separation by gel filtration to ensure the high occupancy as described previously.[3,21] The substrate-bound IDE was crystallized by hanging drop vapor diffusion at 18 °C, using 1 μl of protein (16–20 mg/ml) and 1 μl of mother liquor (10–13% polyethylene glycol monomethyl ether 5000, 100 mM Hepes, pH 7.0, 4–14% Tacsimate, and 10% dioxane). Clusters of needle crystals appeared in 3 to 5 days and were equilibrated in cryo-protective buffer containing 30% glycerol and mother liquor and were flash frozen in liquid nitrogen. Diffraction data were collected at 100 K at the Advance Photon Source 14-BM-C and 19-ID beamlines at Argonne National Laboratory. The data sets were processed using HKL2000.[39] The structures were solved by molecular replacement (Phaser)[40] using the IDE portion of Aβ-bound IDE-E111Q structure as a search model [Protein Data Bank (PDB) code: 2G47[3]]. Structure refinement and rebuilding were performed using REFMAC and Coot.[39,41] The extra electron density at the catalytic chamber of IDE in the structures of IDE in complex with TGF-α, IGF-II, amylin, and Aβ(1–42) were clearly visible based on σ_A-weighted $F_o - F_c$ map calculated by CNS[42] and manually built. The refinement statistics are summarized in Table 2. Figures were generated using PyMOL[43] and CCP4MG.[40] The volumes of the catalytic chamber of IDE and that of insulin were calculated using VOIDOO[44] and shape complementarity was calculated as described previously.[45]

Enzymatic competition assay

Enzyme activities were assayed using a fluorogenic bradykinin-mimetic substrate of IDE, substrate V (7-methoxycoumarin-4yl-acetyl-RPPGFSAFK-2,4-dinitrophenyl; R&D Systems).[3,19–21] Competition reactions were carried out at 37 °C by mixing 90 μl of 0.5 μM substrate V in 50 mM potassium phosphate buffer (pH 7.3) and 10 μl of human IGF-II or TGF-α (Peprotech). The reactions were initiated by the addition of 5 μl of 0.2 mg/ml IDE protein. The substrate V degradation was assessed by monitoring fluorescence intensity for 10 min every 20 s on a Tecan Safire[2] microplate reader (l_{ex} = 327 nm, l_{em} = 395 nm).

Accession codes

The coordinates for IGF-II-, TGF-α-, amylin-, and Aβ(1–42)-bound IDE have been deposited in Research Collaboratory for Structural Bioinformatics PDB under accession codes 3E4Z, 3E50, 3HGZ, and 2WK3, respectively.

Acknowledgements

We are grateful to the staff of the Structural Biology Center and BioCars at the Advanced Photon Source, Argonne National Laboratory, for help in data collection; Erik Johnson for the synthetic Aβ(1–42) peptide; and Ray Hulse for the technical assistance. This work was supported by National Institutes of Health grant GM81539 to W.-J. Tang. Use of the Advanced Photon Source was supported by the U.S. Department of Energy, Office of Basic Energy Sciences, under contract no. W-31-109-ENG-38. Use of the proteomics and informatics services facility was supported by the Chicago Biomedical Consortium.

Supplementary Data

Supplementary data associated with this article can be found, in the online version, at doi:10.1016/j.jmb.2009.10.072

References

1. Malito, E., Hulse, R. E. & Tang, W. J. (2008). Amyloid beta-degrading cryptidases: insulin degrading enzyme, presequence peptidase, and neprilysin. *Cell. Mol. Life Sci.* **65**, 2574–2585.
2. Hulse, R. E., Ralat, L. A. & Tang, W. J. (2009). Structure, function, and regulation of insulin-degrading enzyme. *Vitam. Horm.* **80**, 635–648.
3. Shen, Y., Joachimiak, A., Rosner, M. R. & Tang, W. J. (2006). Structures of human insulin-degrading enzyme reveal a new substrate recognition mechanism. *Nature*, **443**, 870–874.
4. Duckworth, W. C., Bennett, R. G. & Hamel, F. G. (1998). Insulin degradation: progress and potential. *Endocr. Rev.* **19**, 608–624.
5. Johnson, K. A., Bhushan, S., Stahl, A., Hallberg, B. M., Frohn, A., Glaser, E. & Eneqvist, T. (2006). The closed structure of presequence protease PreP forms a unique 10,000 Å^3 chamber for proteolysis. *EMBO J.* **25**, 1977–1986.
6. Taylor, A. B., Smith, B. S., Kitada, S., Kojima, K., Miyaura, H., Otwinowski, Z. *et al.* (2001). Crystal structures of mitochondrial processing peptidase reveal the mode for specific cleavage of import signal sequences. *Structure*, **9**, 615–625.

7. Maskos, K. (2004). Pitrilysins/inverzincins. In *Handbook of Metalloproteins* (Messerschmidt, A., Dode, W. & Cygler, M., eds), vol. 3, pp. 190–198. John Wiley & Sons, Hoboken, NJ.
8. Fawcett, J., Permana, P. A., Levy, J. L. & Duckworth, W. C. (2007). Regulation of protein degradation by insulin-degrading enzyme: analysis by small interfering RNA-mediated gene silencing. *Arch. Biochem. Biophys.* **468**, 128–133.
9. Mirsky, I. A. & Broh-Kahn, R. H. (1949). The inactivation of insulin by tissue extracts; the distribution and properties of insulin inactivating extracts. *Arch. Biochem.* **20**, 1–9.
10. Farris, W., Mansourian, S., Chang, Y., Lindsley, L., Eckman, E. A. & Frosch, M. P. (2003). Insulin-degrading enzyme regulates the levels of insulin, amyloid beta-protein, and the beta-amyloid precursor protein intracellular domain in vivo. *Proc. Natl Acad. Sci. USA*, **100**, 4162–4167.
11. Sladek, R., Rocheleau, G., Rung, J., Dina, C., Shen, L. & Serre, D. (2007). A genome-wide association study identifies novel risk loci for type 2 diabetes. *Nature*, **445**, 881–885.
12. Leissring, M. A., Farris, W., Chang, A. Y., Walsh, D. M., Wu, X., Sun, X. *et al.* (2003). Enhanced proteolysis of beta-amyloid in APP transgenic mice prevents plaque formation, secondary pathology, and premature death. *Neuron*, **40**, 1087–1093.
13. Kurochkin, I. V. (2001). Insulin-degrading enzyme: embarking on amyloid destruction. *Trends Biochem. Sci.* **26**, 421–425.
14. Kim, M., Hersh, L. B., Leissring, M. A., Ingelsson, M., Matsui, T. & Farris, W. (2007). Decreased catalytic activity of the insulin-degrading enzyme in chromosome 10-linked Alzheimer disease families. *J. Biol. Chem.* **282**, 7825–7832.
15. Keller, S., Schmid, C., Zapf, J. & Froesch, E. R. (1989). Inhibition of insulin degradation by insulin-like growth factors I and II in human hepatoma (HepG2) cells. *Acta Endocrinol. (Copenh.)*, **121**, 279–285.
16. Misbin, R. I., Almira, E. C., Duckworth, W. C. & Mehl, T. D. (1983). Inhibition of insulin degradation by insulin-like growth factors. *Endocrinology*, **113**, 1525–1527.
17. Gehm, B. D. & Rosner, M. R. (1991). Regulation of insulin, epidermal growth factor, and transforming growth factor-alpha levels by growth factor-degrading enzymes. *Endocrinology*, **128**, 1603–1610.
18. Muller, D., Baumeister, H., Buck, F. & Richter, D. (1991). Atrial natriuretic peptide (ANP) is a high-affinity substrate for rat insulin-degrading enzyme. *Eur. J. Biochem.* **202**, 285–292.
19. Im, H., Manolopoulou, M., Malito, E., Shen, Y., Zhao, J. & Neant-Fery, M. (2007). Structure of substrate-free human insulin-degrading enzyme (IDE) and biophysical analysis of ATP-induced conformational switch of IDE. *J. Biol. Chem.* **282**, 25453–25463.
20. Malito, E., Ralat, L. A., Manolopoulou, M., Tsay, J. L., Wadlington, N. L. & Tang, W. J. (2008). Molecular bases for the recognition of short peptide substrates and cysteine-directed modifications of human insulin-degrading enzyme. *Biochemistry*, **47**, 12822–12834.
21. Manolopoulou, M., Guo, Q., Malito, E., Schilling, A. B. & Tang, W. J. (2009). Molecular basis of catalytic chamber-assisted unfolding and cleavage of human insulin by human insulin degrading enzyme. *J. Biol. Chem.* **284**, 14177–14188.
22. Roth, R. A., Mesirow, M. L., Yokono, K. & Baba, S. (1984). Degradation of insulin-like growth factors I and II by a human insulin degrading enzyme. *Endocr. Res.* **10**, 101–112.
23. Terasawa, H., Kohda, D., Hatanaka, H., Nagata, K., Higashihashi, N. & Fujiwara, H. (1994). Solution structure of human insulin-like growth factor II; recognition sites for receptors and binding proteins. *EMBO J.* **13**, 5590–5597.
24. Cooke, R. M., Harvey, T. S. & Campbell, I. D. (1991). Solution structure of human insulin-like growth factor 1: a nuclear magnetic resonance and restrained molecular dynamics study. *Biochemistry*, **30**, 5484–5491.
25. Broughton, S. & Partridge, L. (2009). Insulin/IGF-like signalling, the central nervous system and aging. *Biochem. J.* **418**, 1–12.
26. Pollak, M. (2008). Insulin and insulin-like growth factor signalling in neoplasia. *Nat. Rev., Cancer*, **8**, 915–928.
27. Harvey, T. S., Wilkinson, A. J., Tappin, M. J., Cooke, R. M. & Campbell, I. D. (1991). The solution structure of human transforming growth factor alpha. *Eur. J. Biochem.* **198**, 555–562.
28. Kohda, D. & Inagaki, F. (1992). Three-dimensional nuclear magnetic resonance structures of mouse epidermal growth factor in acidic and physiological pH solutions. *Biochemistry*, **31**, 11928–11939.
29. Schneider, M. & Wolf, E. (2009). The epidermal growth factor receptor ligands at a glance. *J. Cell. Physiol.* **218**, 460–466.
30. Haataja, L., Gurlo, T., Huang, C. J. & Butler, P. C. (2008). Islet amyloid in type 2 diabetes, and the toxic oligomer hypothesis. *Endocr. Rev.* **29**, 303–316.
31. Höppener, J. W., Ahrén, B. & Lips, C. J. (2000). Islet amyloid and type 2 diabetes mellitus. *N. Engl. J. Med.* **343**, 411–419.
32. Baker, N. A., Sept, D., Joseph, S., Holst, M. J. & McCammon, J. A. (2001). Electrostatics of nanosystems: application to microtubules and the ribosome. *Proc. Natl Acad. Sci. USA*, **98**, 10037–10041.
33. Chothia, C., Lesk, A. M., Dodson, G. G. & Hodgkin, D. C. (1983). Transmission of conformational change in insulin. *Nature*, **302**, 500–505.
34. Moy, F. J., Li, Y. C., Rauenbuehler, P., Winkler, M. E., Scheraga, H. A. & Montelione, G. T. (1993). Solution structure of human type-alpha transforming growth factor determined by heteronuclear NMR spectroscopy and refined by energy minimization with restraints. *Biochemistry*, **32**, 7334–7353.
35. Torres, A. M., Forbes, B. E., Aplin, S. E., Wallace, J. C., Francis, G. L. & Norton, R. S. (1995). Solution structure of human insulin-like growth factor II. Relationship to receptor and binding protein interactions. *J. Mol. Biol.* **248**, 385–401.
36. Hamel, F. G., Gehm, B. D., Rosner, M. R. & Duckworth, W. C. (1997). Identification of the cleavage sites of transforming growth factor alpha by insulin-degrading enzymes. *Biochim. Biophys. Acta*, **1338**, 207–214.
37. Leissring, M. A., Lu, A., Condron, M. M., Teplow, D. B., Stein, R. L., Farris, W. & Selkoe, D. J. (2003). Kinetics of amyloid beta-protein degradation determined by novel fluorescence- and fluorescence polarization-based assays. *J. Biol. Chem.* **278**, 37314–37320.
38. Felder, C. E., Prilusky, J., Silman, I. & Sussman, J. L. (2007). A server and database for dipole moments of proteins. *Nucleic Acids Res.* **35**, W512–521.
39. Murshudov, G. N., Vagin, A. A. & Dodson, E. J. (1997). Refinement of macromolecular structures by the maximum-likelihood method. *Acta Crystallogr., Sect. D: Biol. Crystallogr.* **53**, 240–255.

40. Potterton, E., McNicholas, S., Krissinel, E., Cowtan, K. & Noble, M. (2002). The CCP4 molecular-graphics project. *Acta Crystallogr., Sect. D: Biol. Crystallogr.* **58**, 1955–1957.
41. Emsley, P. & Cowtan, K. (2004). Coot: model-building tools for molecular graphics. *Acta Crystallogr., Sect. D: Biol. Crystallogr.* **60**, 2126–2132.
42. Brunger, A. T., Adams, P. D., Clore, G. M., DeLano, W. L., Gros, P. & Grosse-Kunstleve, R. W. (1998). Crystallography & NMR system: a new software suite for macromolecular structure determination. *Acta Crystallogr., Sect. D: Biol. Crystallogr.* **54**, 905–921.
43. Delano, W. L. (2002). PyMOL. Pymol.sourceforge.net.
44. Kleywegt, G. J. & Jones, T. A. (1994). Detection, delineation, measurement and display of cavities in macromolecular structures. *Acta Crystallogr., Sect. D: Biol. Crystallogr.* **50**, 178–185.
45. Lawrence, M. C. & Colman, P. M. (1993). Shape complementarity at protein/protein interfaces. *J. Mol. Biol.* **234**, 946–950.